

Scale-dependent Error Growth in Navier–Stokes Simulations

Nazmi Burak Budanur and Holger Kantz

Max Planck Institute for the Physics of Complex Systems (MPIPKS)

Nöthnitzer Straße 38, 01187 Dresden, Germany

September 5, 2022

Abstract

We estimate the maximal Lyapunov exponent at different resolutions and Reynolds numbers in large eddy (LES) and direct numerical simulations (DNS) of sinusoidally-driven Navier–Stokes equations in three dimensions. Independent of the Reynolds number when nondimensionalized by Kolmogorov units, the LES Lyapunov exponent diverges as an inverse power of the effective grid spacing showing that the fine scale structures exhibit much faster error growth rates than the larger ones. Effectively, i.e., ignoring the cut-off of this phenomenon at the Kolmogorov scale, this behavior introduces an upper bound to the prediction horizon that can be achieved by improving the precision of initial conditions through refining of the measurement grid.

1 Introduction

A defining feature of deterministic chaos is that infinitesimal errors in the initial conditions grow, on average, exponentially fast in time, the rate being called the maximal Lyapunov exponent λ of the system. This is a challenge to predictions and often attributed to the difficulties in weather forecasting since the initial condition which one plugs into some model equations will represent the reality only up to some inaccuracy and even if the model were perfect, the initial error ϵ_0 would grow approximately as $\epsilon(t) \approx \epsilon_0 e^{\lambda t}$. At latest when the distance between this forecast trajectory and the unknown “true” trajectory of the system reaches the order of magnitude of the attractor size (or, more pragmatically, the standard deviation of the quantity to be forecast), this forecast has lost its usefulness, and the prediction horizon is reached. This exponential error growth is already quite unfavorable if one wants to extend the prediction horizon: for a linear extension δt of the latter, the initial inaccuracy has to be reduced exponentially by a factor of $e^{-\lambda \delta t}$.

Since the 1950s, several authors [1–8] have argued that the practical situation in forecasting hydrodynamic systems is likely to be much worse when a range of spatial and temporal scales are at present as in the case of turbulent flows [9, 10]. The basic idea is that for a multi-scale hydrodynamic system, refining the initial conditions would necessarily translate

to the inclusion of small-scale motions into the model, which in turn have shorter characteristic temporal scales, such as the eddy turnover time [11], thus resulting in faster-growing errors. While [1–8] differ in many aspects such as the systems and models that they consider, their common conclusion is that the predictability in hydrodynamic systems is much more strongly limited than by the simple exponential divergence of trajectories as a result of the described phenomenon, which hereafter we refer to as *scale-dependent error growth*.

Evidence of scale-dependent error growth has also been reported in the models of atmosphere: In [12], fast-growth of errors at small-scales was found in the Global Forecast System of the National Centers for Environmental Prediction, and more recently in [13] for ensemble forecasts of the European Centre for Medium-Range Weather Forecasts. In [14], it was argued that the results of [12] were compatible with the power-law divergence of the finite-size Lyapunov exponent in vanishing amplitude of the initial error. Altogether, these results point to a significant role of scale-dependent error growth for weather forecasts.

The above-cited papers on scale-dependent error growth consider forecast scenarios in which one is interested in predicting large-scale motions in the system which are assumed to be measured with high accuracy and asks “How long will it take for the uncertainties in unresolved length scales to contaminate those of interest?” This question differs fundamentally from that of the standard exponential divergence of infinitesimal errors as it is concerned with finite-size deviations. Motivated by this, Aurell et al. [6] introduced the concept of finite size Lyapunov exponents and applied it to a shell model turbulence cascade. By computing the error doubling times for perturbations of a finite size E and averaging over the system’s attractor, they concluded that the rate $\lambda_F(E)$ of error growth can be well described by a power law $\lambda_F(E) \propto E^{-\beta}$ with $\beta > 0$. Later, Boffetta and Musacchio [8] presented numerical evidence for this kind of error growth behavior in the direct numerical simulations (DNS) of homogeneous isotropic turbulence.

In this paper, we present simulation results which demonstrate that the scale-dependent error growth is already relevant for the growth rate of infinitesimal perturbations in hydrodynamic models with varying resolutions. In order to understand how inclusion of smaller scales affects the rate of error growth, we perform large eddy simulations (LES) at different resolutions, wherein the motions at length scales smaller than the grid spacing are explicitly filtered out. In these, we estimate the maximal Lyapunov exponents and compare to those we find in the fully-resolved direct numerical simulations (DNS). Our results confirm that increasing the spatial resolution of LES indeed results in faster-growing errors. Moreover, when normalized by the Kolmogorov length and time scales, the rates of error growth at different Reynolds numbers and resolutions collapse on a single curve that can be fit by a power law. Finally, we consider a forecast scenario where the error on the initial state’s measurement is proportional to the grid spacing of LES and show that scale-dependent error growth yields an upper limit for the maximal prediction horizon that can be achieved through LES.

2 Computational setup

Let us denote the three-dimensional cartesian coordinates by (x_1, x_2, x_3) and the partial derivatives with respect to time t and x_i as ∂_t and ∂_i , respectively. Adopting also the

summation convention over the repeated indices, the filtered Navier–Stokes equations read

$$\partial_t u_j = -u_i \partial_i u_j - \partial_j p + 2\partial_i (Re^{-1} + \nu_T) S_{ij} + f_j, \quad (1)$$

where u_j are the velocity field components subjected to the incompressibility $\partial_j u_j = 0$ and periodic boundary conditions $u_j|_{x_i+L_i} = u_j|_{x_i}$, Re is the Reynolds number, $S_{ij} = (\partial_i u_j + \partial_j u_i)/2$ is the rate-of-strain tensor, $f_j = (4Re)^{-1} \sin(2\pi x_2/L_2) \delta_{1j}$ is a sinusoidal body force, and ν_T is the so-called “eddy viscosity” that aims to account for the transfer of energy to the length scales below a resolution. We implement the Smagorinsky model [15]

$$\nu_T = (C_S \Delta)^2 \sqrt{S_{ij} S_{ij}}, \quad (2)$$

where C_S is the Smagorinsky constant and Δ is the length scale below which the motion is not resolved. Note that the full Navier–Stokes equations corresponding to the three-dimensional Kolmogorov flow [16] are recovered in (1) if $\nu_T = 0$.

We simulate (1) using `dnsbox` [17, 18] which discretizes the velocity field u_i using Fourier series in all three directions, compute the nonlinear terms in (1) pseudospectrally [19] and time-step the equations using a semi-implicit second-order predictor-corrector scheme. All of our simulations are carried out in a cubic domain with the edge length $L_i = 4$, yielding the laminar solution of (1) when $\nu_T = 0$ as $u_j = \sin(\pi x_2/2) \delta_{1j}$. The laminar solution with a unit peak amplitude at $x_2 = 1$ sets our length and velocity scales, thus the time scale as their ratio.

Table 1 shows a summary of our simulation domains. For the DNS domains, we determine our resolutions n^{DNS} such that the grid spacing L_i/n^{DNS} is on the order of the Kolmogorov length scale $\eta = (Re^3 \varepsilon)^{-1/4}$, where ε is the rate of turbulence dissipation. We estimate this as $\varepsilon = Re^{-1} \langle \partial_j \tilde{u}_i \partial_j \tilde{u}_i \rangle$ where \tilde{u}_i are the fluctuating velocity components with means along the homogeneous directions x_1 and x_3 subtracted and the angle brackets indicate the average over simulation domain. Besides the Re based on the laminar solution, in Table 1 we also report $Re_{rms} = \langle \tilde{u} \rangle_{rms} L_i Re$ and $Re_T = \langle \tilde{u} \rangle_{rms} l_T Re$ where $\langle \tilde{u} \rangle_{rms}$ is the root mean square of the fluctuating velocity and $l_T = \sqrt{15/(\varepsilon Re)} \langle \tilde{u} \rangle_{rms} Re$ is the Taylor microscale [11]. Our final estimates of η , Re_{rms} and Re_T come from an average of it over 10 fluid states in each DNS domain. We started our simulations with a variable time-step that keeps the Courant–Friedrichs–Lewy number approximately equal to 0.25, once a state on the attractor is reached, we fix our time step to $\Delta t = 0.04$ in DNS and $\Delta t = 0.02$ in LES domains.

Table 1: Properties of the simulation domains. In all LES simulations the Smagorinsky constant was set to $C_S = 0.1$. $\min n^{LES}$ and $\max n^{LES}$ corresponds to the smallest and the largest number of grid points used in LES at the corresponding Re . $k_{max} = 2\pi(n^{DNS}/2+1)/L_i$ is the largest resolved wave number in each direction.

Re	Re_{rms}	Re_T	$\min n^{LES}$	$\max n^{LES}$	n^{DNS}	$k_{max}\eta$
10,000	460.41 \pm 45.80	30.07 \pm 4.41	24	80	216	4.07
20,000	696.53 \pm 57.34	38.45 \pm 4.16	24	96	240	3.39
30,000	866.35 \pm 78.90	41.60 \pm 3.41	24	112	288	3.41
40,000	1,006.55 \pm 72.88	45.14 \pm 4.15	24	128	320	3.39
80,000	1,412.58 \pm 94.68	54.19 \pm 6.30	24	144	432	3.58

Let $\mathbf{u}(t)$ be the fluid state at time t , Φ^t denote the time- t map induced by the dynamics transforming $\mathbf{u}(t)$ as $\mathbf{u}(t) = \Phi^t(\mathbf{u}(0))$, and $\|\cdot\|$ indicate the L_2 norm $\|\mathbf{u}\| = (L_1 L_2 L_3)^{-1} \int \int \int u_i u_i d^3x$. We estimate the maximal Lyapunov exponents via Benettin algorithm [20] through the following steps. Starting from an initial state $\mathbf{u}(0)$ on the attractor, we add a random perturbation $\delta\mathbf{u}(0)$ with $\|\delta\mathbf{u}(0)\| = \sigma\|\mathbf{u}(0)\|$, where σ is a small positive real number, to this state and simulate $\mathbf{u}(t)$ and $\mathbf{u}(t) + \delta\mathbf{u}(t)$ in parallel. At each τ , we rescale $\delta\mathbf{u}(n\tau)$ such that its norm is set as $\|\delta\mathbf{u}(n\tau)\| = \sigma\|\mathbf{u}(n\tau)\|$ where $n = 1, 2, \dots$. After some transient time $t_{trans} = n_t\tau$, we estimate the maximal Lyapunov exponent as

$$\lambda \approx \frac{1}{N\tau} \sum_{n=n_t}^{n_t+N} \ln \frac{\|\Phi^\tau(\mathbf{u}(n\tau) + \delta\mathbf{u}(n\tau)) - \Phi^\tau(\mathbf{u}(n\tau))\|}{\|\delta\mathbf{u}(n\tau)\|}. \quad (3)$$

For our numerical results to follow, we used $\sigma = 10^{-4}$, $t_{trans} = 400$, and $\tau = 20$ in DNS and $\sigma = 10^{-4}$, $t_{trans} = 400$, and $\tau = 5$ in LES. We confirmed that our results are insensitive to these parameter choices by partially reproducing them using σ one order of magnitude up and down; and Δt at half and double of its value.

3 Results

Figure 1A shows the numerical estimates of the largest Lyapunov exponent obtained in DNS at five different Re as straight lines, and the resolution-dependent exponents obtained in LES at the same set of Res against $1/\Delta$. Shown values are obtained by averaging over the estimates of the final 1000 time units in each simulation and the widths of error bars and shaded regions in Figure 1 correspond to two standard deviations. We observe that as the LES resolution is increased, so does the Lyapunov exponent with a clear trend towards the corresponding exponent from DNS. Note that the decrease of Lyapunov exponents as Re is increased is due to our nondimensionalization of the system through the sinusoidal laminar solution of the Kolmogorov flow. When we rescale the Lyapunov exponents, which are measured in inverse time units, by the Kolmogorov time $\tau_\eta = (Re\varepsilon)^{-1/2}$, and plot them against the LES grid spacing Δ normalized by the the Kolmogorov length η , we obtain the data collapse shown in Figure 1B. Hence, the Reynolds-number dependence is fully accounted for by the Reynolds-number dependence of the Kolmororov time and length scale. The larger uncertainties in Figure 1B with respect to those in Figure 1A are due to the standard deviations of our estimates of η and τ , which we compute as an ensemble average over turbulent DNS states.

Figure 2A shows the shell-averaged energy spectra of turbulence obtained as an ensemble average over 10 states in each DNS domain and the reported uncertainties are one standard deviation. Following [21], we replotted these spectra in Figure 2B in Kolmogorov units to show that they collapse at large wave numbers (small scales). As we compute the Lyapunov exponent, we expect the perturbations $\delta\mathbf{u}$ to align with the most unstable direction of the system, i.e. the leading Lyapunov vector. Taking these as an approximation to the leading Lyapunov vector, we plotted their energy spectra in Figure 2C. Similar to the flow states, when we rescale these spectra by $(\eta Re)^2$ and plot against the wave numbers premultiplied by η , we observe that they similarly collapse onto a single curve. These suggest that the scaling

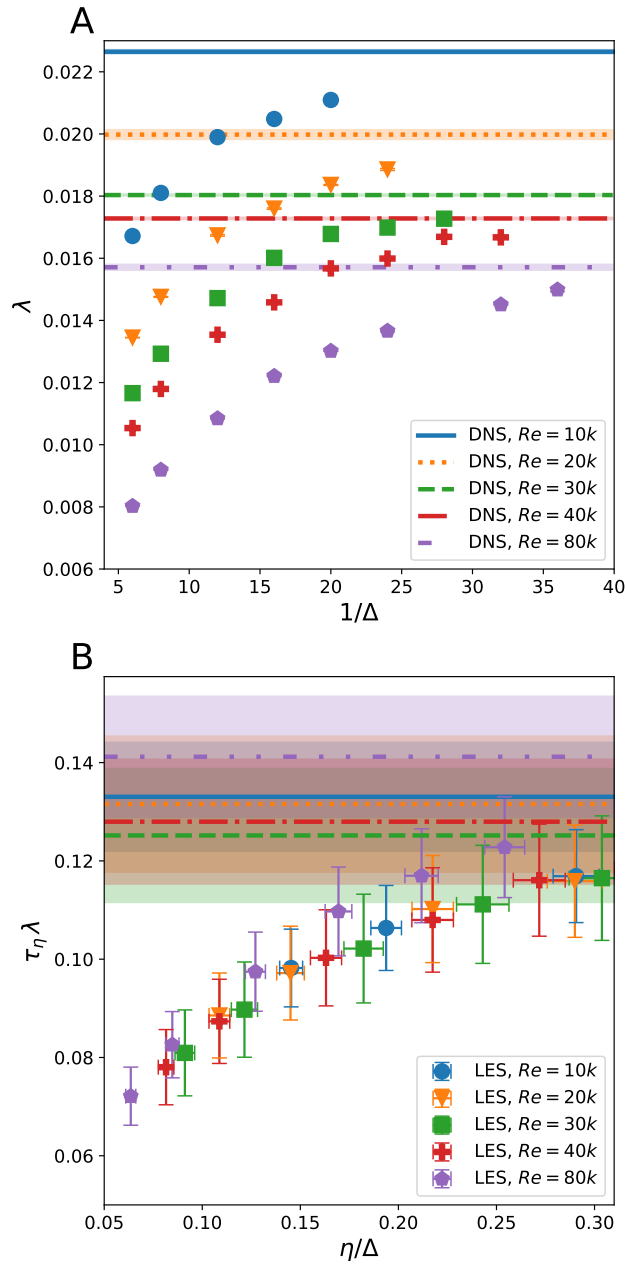


Figure 1: (color online) **A**. Maximal Lyapunov exponent estimated in LES at different resolutions. Fully-resolved DNS Lyapunov exponents are indicated by horizontal lines. **B**. Same as A, scaled by Kolmogorov length and time scales. Legends in A and B apply to both panels.

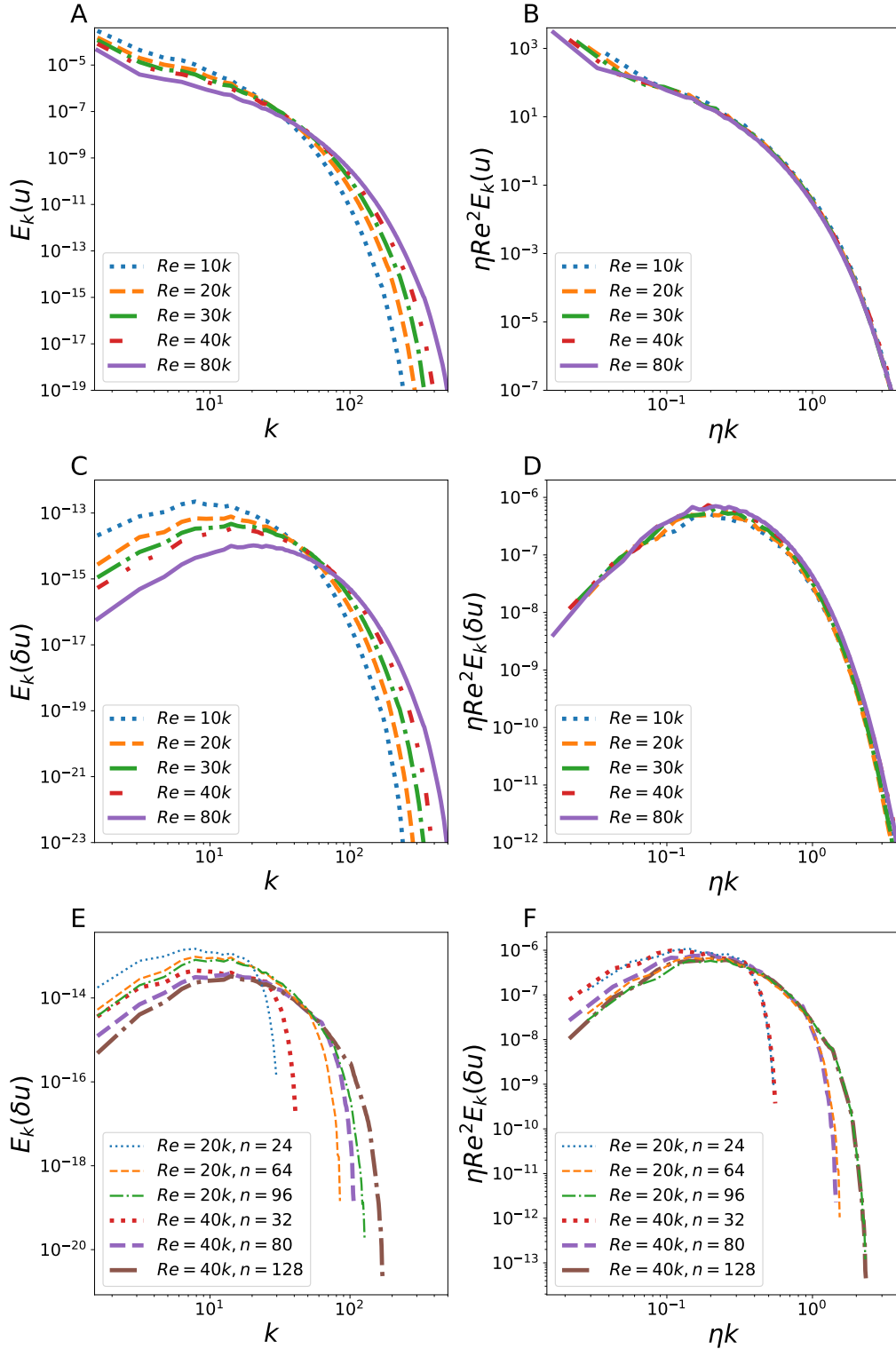


Figure 2: (color online) **A.** Shell-averaged energy spectra of turbulence in DNS. **B.** Same as A, in Kolmogorov units. **C.** Shell-averaged energy spectra of the Lyapunov vectors in DNS. **D.** Same as C, in Kolmogorov units. **E.** Shell-averaged energy spectra of the Lyapunov vectors in LES at $Re = 20,000$ and $Re = 40,000$ for a select subset of the cutoff resolutions. **F.** Same as E, in Kolmogorov units.

of the Lyapunov exponents with Kolmogorov time τ_η can be attributed to the small-scale universality of turbulence [22]. As shown in Figure 2E and F, we observe a similar collapse of the energy spectra for Lyapunov vectors when we compare domains whose resolutions match one another in Kolmogorov units. We chose the Re and resolutions for Figure 2E and F by noting that $\eta|_{Re=20,000}/\eta|_{Re=40,000} \approx 1.3$ is also approximately equal to the ratio of number of grid points, i.e. $32/24 \approx 80/64 \approx 128/96 \approx 1.3$. In other words, the energy spectra of Lyapunov vectors in two LES simulations at different Re are nearly identical when we use the same LES resolution in units of η .

Having obtained the scaling of the LES Lyapunov exponents in Kolmogorov units, we replot our data as a function of the gridspacing Δ along with a power law fit in Figure 3 A and B in linear and log-log scales, respectively. In Figure 3 and the rest of this article, all lengths and times are given in Kolmogorov units. The largest Lyapunov exponent obtained by LES of different spatial resolutions Δ as a function of the latter is well described by a power law

$$\lambda(\Delta) = \alpha\Delta^{-\rho} \quad (4)$$

where $\alpha \approx 0.18$ and $\rho \approx 0.32$. This is the central result: The smaller are the spatial scales that the perturbation fields $\delta\mathbf{u}$ can contain, the faster are their growth rates. This is also reflected in Figure 2F, where it can be seen that increasing the resolution of LES results in more and more energy in the small-scales of the Lyapunov vectors' energy spectra. Note, also that as the LES resolution is increased, the spectra of the Lyapunov vectors in Figure 2F better approximates those obtained in DNS which are shown in Figure 2D.

In the limit $\Delta \rightarrow 0$, (4) with $\rho > 0$ yields $\lambda \rightarrow \infty$. Of course, this limit is an unphysical one since (4) is only valid for $\Delta \gg \eta$. Nevertheless by examining it, we can derive an upper bound for the prediction horizon that can be achieved by LES. Let us imagine a forecast scenario where the initial state of the fluid is determined using a measurement grid with spacing Δ and modeled with an LES of the same resolution. In such a setup, it is reasonable to assume that the initial errors of our measurement will be proportional to Δ , i.e. $\epsilon_0 = \gamma\Delta$, where γ accounts for all the other factors that contribute to the initial error, for instance temporal resolution, which we assume to remain unchanged. Exponential growth of this initial error for some time t with the Lyapunov exponent (4) yields

$$\epsilon(t) = \gamma\Delta e^{\alpha\Delta^{-\rho}t}, \quad (5)$$

which we can solve for the prediction horizon t_{pred} to reach a maximum tolerable ϵ_{th} as

$$t_{pred} = \frac{\Delta^\rho}{\alpha} [\ln \epsilon_{th} - \ln(\gamma\Delta)]. \quad (6)$$

This is the standard expression for the prediction horizon with Δ^ρ/α and $\gamma\Delta$ taking the role of the Lyapunov time and the initial error, respectively. Note that when $\Delta \rightarrow 0$ we get $t_{pred} = 0$ due to the vanishing of the Lyapunov time, which already tells us decreasing the grid spacing Δ might not necessarily translate to an extended prediction horizon. Under which condition this is the case is given by the derivative

$$\frac{dt_{pred}}{d\Delta} = \frac{\Delta^{\rho-1}}{\alpha} \left[\rho \ln \frac{\epsilon_{th}}{\gamma\Delta} - 1 \right], \quad (7)$$

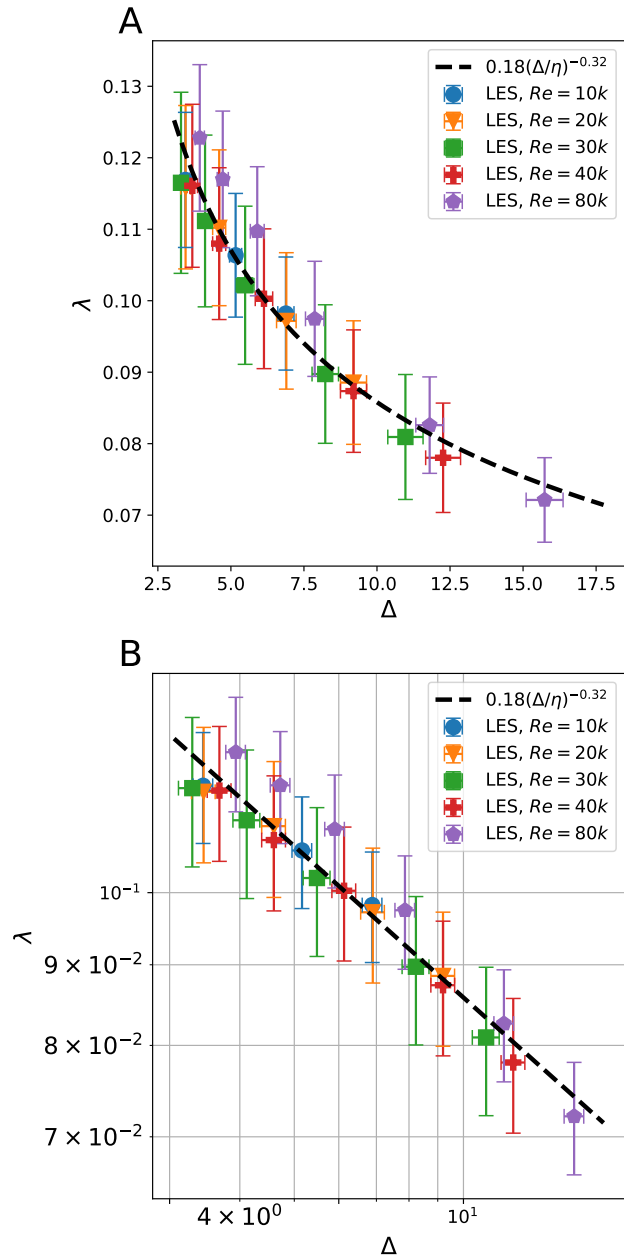


Figure 3: (color online) **A.** Maximal Lyapunov exponents in LES as a function of grid spacing in Kolmogorov units along with the best-fit power law. **B.** Log-log plot of the same data.

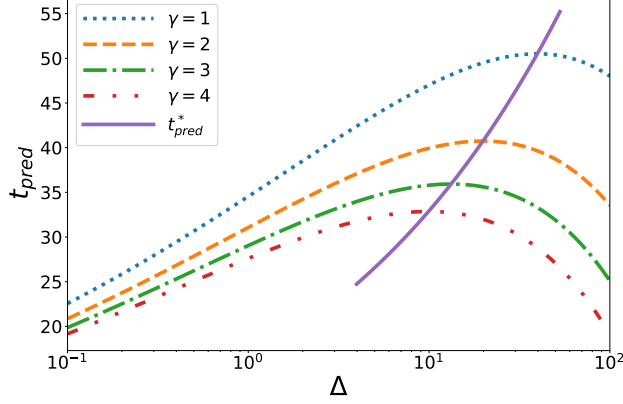


Figure 4: (color online) Prediction horizon (6) as a function of grid spacing plotted for $\gamma = \{1, 2, 3, 4\}$ and $\epsilon_{th} = 1000$.

which is negative when $\epsilon_{th}/(\gamma\Delta) < e^{1/\rho}$ and the equality gives the point of diminishing returns because if $dt_{pred}/d\Delta > 0$, then reducing Δ results in a shorter prediction horizon. Consequently, the optimal resolution is given by the 0 of (7) as

$$\Delta^* = \frac{\epsilon_{th}}{e^{1/\rho}\gamma} \quad (8)$$

Plugging it into (6), we get the maximal prediction horizon

$$t_{pred}^* = \frac{\epsilon_{th}^\rho}{e\alpha\rho\gamma^\rho}. \quad (9)$$

We illustrate (6) in Figure 4 where we plotted it as a function of Δ for $\epsilon_{th} = 1000$ (arbitrary) and $\gamma = 1, 2, 3, 4$ along with t^* indicating the maximal prediction horizon as a function of γ . In the light of our results, t^* given by (9) is the longest prediction horizon that is achievable through LES, if the magnitude of initial uncertainties is proportional to the LES grid spacing Δ and $\Delta \gg \eta$, i.e. the LES grid is much coarser than the Kolmogorov length. This can be straightforwardly generalized to initial errors that scale differently with the grid spacing, i.e. $\epsilon_0 = \gamma\Delta^\mu$, with $\mu > 0$. Following steps analogous to (5–7), we get the derivative of prediction horizon with respect to the grid spacing for this case as

$$\frac{dt_{pred}(\mu)}{d\Delta} = \frac{\Delta^{\rho-1}}{\alpha} \left[\rho \ln \frac{\epsilon_{th}}{\gamma\Delta} - \mu \right], \quad (10)$$

which is negative as long as $\epsilon_{th}/(\gamma\Delta) < e^{\mu/\rho}$. Thus, in principle, the prediction horizon can be extended by ensuring this condition if $\mu > 1$ is technologically possible. Conversely, if reducing the grid spacing results in a slower-than-linear improvement ($\mu < 1$) of the initial condition's precision, then the point of diminishing returns is reached earlier.

4 Conclusion

In view of weather forecasting, this might have severe implications for the limits of predictions. Numerical weather prediction models and atmospheric general circulation models (AGCMs)

contain the Navier–Stokes equations in some form as the core for modeling atmospheric transport [23, 24] among the so-called primitive equations. For better resolution of small scale atmospheric processes with the ultimate goal to model convection and clouds, the grid spacing in weather models has been reduced according to compute power availability and is currently down to, e.g., 2.2km in the high-resolution DWD model for Germany[25]. It is well known by practitioners that high-resolution models lose their predictability on their small scales much faster than coarser models do on their respective scales, and consequently high resolution models are used for short term forecasts only (e.g., DWD limits the forecast runs of ICON-D2 to 27 hours). Our finding of an optimal resolution for maximising the prediction horizon sets this empirics into a broader context and shows that forecast horizon cannot be extended by simply improving resolution alone.

Scaling of the maximal Lyapunov exponents of a turbulent flow with the Kolmogorov time scale was conjectured in [26], assumed in the subsequent literature [6] and recently con- tested in homogeneous isotropic turbulence simulations [8, 27, 28]. While our results are in agreement with the conjecture, thus at odds with the results of [8, 27, 28], we cannot rule out subtle variations or finite- Re effects on this scaling based on the present results. We would like to note, however, two important differences between the cited studies and the present one. Firstly, the resolution of simulations we perform are roughly twice the ones in [8, 27, 28]. We chose to perform DNS at resolutions much higher than the traditional turbulence literature following the findings of [22, 29] which emphasized importance of resolving the Kolmogorov scale for observing the small-scale universality in simulations. The other potential explanation of the apparent discrepancy is [8, 27, 28]’s use of Machiel’s [30] forcing which is a positive feedback on the large scales. Although irrelevant for small scales, such a forcing term could make the large scales artificially unstable and result in an unex- pected behavior of the Lyapunov exponents. Another recent paper [31] computing Lyapunov exponents in LES and DNS of homogeneous isotropic turbulence reported a DNS estimate $\lambda\tau_\eta \approx 0.122$, which is within the error bars of our results in Figure 1, suggesting a universal behavior of the maximal Lyapunov exponent. Altogether, we believe that further research is necessary for settling the question whether the maximal Lyapunov exponent in turbulence indeed scales with the Kolmogorov time.

In summary, we studied the rate of error growth in LES and DNS of sinusoidally forced Navier–Stokes equations in three-dimensions at different Reynolds numbers and LES reso- lutions. We found that independent of the Reynolds number in the turbulent regime, the largest Lyapunov exponent is a fixed multiple of the inverse Kolmogorov time in DNS, and the LES exponents at different Re collapse onto a single curve that can be approximated by a power law when nondimensionalized using Kolmogorov units. Using this power law as a phenomenological model of the scale-dependent error growth, we showed that in a forecast scenario where initial errors are proportional to the resolution cutoff, the scale dependent error growth introduces an upper limit to the achievable prediction horizon. While the exact functional dependence and the numerical values of LES Lyapunov exponents are likely to depend on the studied models, we expect the scale-dependent error growth to be a common feature of turbulence since it appears to be related to the small scales, at which turbulent flows exhibit universality [22]. We thus believe that scale-dependent error growth should be taken into consideration in forecast scenarios where hydrodynamic transport is modelled.

Acknowledgments. We gratefully acknowledge the computing resources provided by the

References

- [1] P. D. Thompson. Uncertainty of initial state as a factor in the predictability of large scale atmospheric flow patterns. *Tellus*, 9(3):275–295, aug 1957. doi: 10.3402/tellusa.v9i3.9111. URL <https://doi.org/10.3402/tellusa.v9i3.9111>.
- [2] E. N. Lorenz. The predictability of a flow which possesses many scales of motion. *Tellus*, 21(3):289–307, jun 1969. doi: 10.1111/j.2153-3490.1969.tb00444.x. URL <https://doi.org/10.1111%2Fj.2153-3490.1969.tb00444.x>.
- [3] G. D. Robinson. Some current projects for global meteorological observation and experiment. *Q. J. R. Meteorol. Soc.*, 93(398):409–418, oct 1967. doi: 10.1002/qj.49709339802. URL <https://doi.org/10.1002%2Fqj.49709339802>.
- [4] G. D. Robinson. The predictability of a dissipative flow. *Q. J. R. Meteorol. Soc.*, 97(413):300–312, jul 1971. doi: 10.1002/qj.49709741305. URL <https://doi.org/10.1002%2Fqj.49709741305>.
- [5] C. E. Leith and R. H. Kraichnan. Predictability of turbulent flows. *J. Atmos. Sci.*, 29(6):1041 – 1058, 1972. doi: 10.1175/1520-0469(1972)029<1041:POTF>2.0.CO;2. URL https://journals.ametsoc.org/view/journals/atasc/29/6/1520-0469_1972_029_1041_potf_2_0_co_2.xml.
- [6] E. Aurell, G. Boffetta, A. Crisanti, et al. Growth of noninfinitesimal perturbations in turbulence. *Phys. Rev. Lett.*, 77(7):1262–1265, aug 1996. doi: 10.1103/physrevlett.77.1262. URL <https://doi.org/10.1103%2Fphysrevlett.77.1262>.
- [7] R. Rotunno and C. Snyder. A generalization of Lorenz’s model for the predictability of flows with many scales of motion. *J. Atmos. Sci.*, 65(3):1063–1076, mar 2008. doi: 10.1175/2007jas2449.1. URL <https://doi.org/10.1175%2F2007jas2449.1>.
- [8] G. Boffetta and S. Musacchio. Chaos and predictability of homogeneous-isotropic turbulence. *Phys. Rev. Lett.*, 119(5), aug 2017. doi: 10.1103/physrevlett.119.054102. URL <https://doi.org/10.1103%2Fphysrevlett.119.054102>.
- [9] L. F. Richardson and P. Lynch. *Weather Prediction by Numerical Process*. Cambridge University Press, 2007. doi: 10.1017/cbo9780511618291. URL <https://doi.org/10.1017%2Fcbo9780511618291>.
- [10] A. Kolmogorov. The local structure of turbulence in incompressible viscous fluid for very large reynolds numbers. *Proc. R. Soc. A*, 434(1890):9–13, jul 1991. doi: 10.1098/rspa.1991.0075. URL <https://doi.org/10.1098%2Frspa.1991.0075>.
- [11] S. B. Pope. *Turbulent Flows*. Cambridge University Press, aug 2000. doi: 10.1017/cbo9780511840531. URL <https://doi.org/10.1017%2Fcbo9780511840531>.

- [12] J. Harlim, M. Oczkowski, J. A. Yorke, et al. Convex error growth patterns in a global weather model. *Phys. Rev. Lett.*, 94(22), jun 2005. doi: 10.1103/physrevlett.94.228501. URL <https://doi.org/10.1103%2Fphysrevlett.94.228501>.
- [13] H. Bednář and H. Kantz. Prediction error growth in a more realistic atmospheric toy model with three spatiotemporal scales. *Geosci. Model Dev. Discuss.*, 2021:1–27, 2021. doi: 10.5194/gmd-2021-256. URL <https://gmd.copernicus.org/preprints/gmd-2021-256/>.
- [14] J. Brisch and H. Kantz. Power law error growth in multi-hierarchical chaotic systems—a dynamical mechanism for finite prediction horizon. *New J. Phys.*, 21(9):093002, sep 2019. doi: 10.1088/1367-2630/ab3b4c. URL <https://doi.org/10.1088%2F1367-2630%2Fab3b4c>.
- [15] J. Smagorinsky. General circulation experiments with the primitive equations: I. the basic experiment. *Mon. Weather Rev.*, 91(3):99–164, 1963. doi: 10.1175/1520-0493(1963)091<0099:GCEWTP>2.3.CO;2. URL [https://doi.org/10.1175/1520-0493\(1963\)091<0099:GCEWTP>2.3.CO;2](https://doi.org/10.1175/1520-0493(1963)091<0099:GCEWTP>2.3.CO;2).
- [16] J. V. Shebalin and S. L. Woodruff. Kolmogorov flow in three dimensions. *Phys. Fluids*, 9(1):164–170, jan 1997. doi: 10.1063/1.869159. URL <https://doi.org/10.1063%2F1.869159>.
- [17] G. Yalnız, B. Hof, and N. B. Budanur. Coarse graining the state space of a turbulent flow using periodic orbits. *Phys. Rev. Lett.*, 126(24), jun 2021. doi: 10.1103/physrevlett.126.244502. URL <https://doi.org/10.1103%2Fphysrevlett.126.244502>.
- [18] G. Yalnız and N. B. Budanur. dnsbox, 2021. URL <https://github.com/burakbudanur/dnsbox>. github.com/burakbudanur/dnsbox.
- [19] C. Canuto, A. Quarteroni, M. Y. Hussaini, and T. A. Zang. *Spectral Methods*. Springer Berlin Heidelberg, 2007. doi: 10.1007/978-3-540-30728-0. URL <https://doi.org/10.1007%2F978-3-540-30728-0>.
- [20] G. Benettin, L. Galgani, A. Giorgilli, and J. Strelcyn. Lyapunov characteristic exponents for smooth dynamical systems and for hamiltonian systems; a method for computing all of them. part 1: Theory. *Meccanica*, 15(1):9–20, mar 1980. doi: 10.1007/bf02128236. URL <https://doi.org/10.1007%2Fbf02128236>.
- [21] R. T. Cerbus, C. Liu, G. Gioia, and P. Chakraborty. Small-scale universality in the spectral structure of transitional pipe flows. *Science Advances*, 6(4), jan 2020. doi: 10.1126/sciadv.aaw6256. URL <https://doi.org/10.1126%2Fsciadv.aaw6256>.
- [22] J. Schumacher, J. D. Scheel, D. Krasnov, et al. Small-scale universality in fluid turbulence. *Proc. Natl. Acad. Sci. U.S.A.*, 111(30):10961–10965, jul 2014. doi: 10.1073/pnas.1410791111. URL <https://doi.org/10.1073%2Fpnas.1410791111>.
- [23] J. Coiffier. *Fundamentals of Numerical Weather Prediction*. Cambridge University Press, 2011.

- [24] T. T. Warner. *Numerical Weather and Climate Prediction*. Cambridge University Press, 2017.
- [25] DWD. NWP forecast data, viewed on Feb. 14, 2022. URL https://www.dwd.de/EN/ourservices/nwp_forecast_data/nwp_forecast_data.html.
- [26] D. Ruelle. Microscopic Fluctuations and Turbulence. In *Turbulence, Strange Attractors and Chaos*, pages 193–194. World Scientific, sep 1995. doi: 10.1142/9789812833709_0010. URL https://doi.org/10.1142/9789812833709_0010.
- [27] P. Mohan, N. Fitzsimmons, and R. D. Moser. Scaling of Lyapunov exponents in homogeneous isotropic turbulence. *Phys. Rev. Fluids*, 2(11), nov 2017. doi: 10.1103/physrevfluids.2.114606. URL <https://doi.org/10.1103/physrevfluids.2.114606>.
- [28] A. Berera and R. D. Ho. Chaotic properties of a turbulent isotropic fluid. *Phys. Rev. Lett.*, 120(2), jan 2018. doi: 10.1103/physrevlett.120.024101. URL <https://doi.org/10.1103/physrevlett.120.024101>.
- [29] D. A. Donzis, P. K. Yeung, and K. R. Sreenivasan. Dissipation and enstrophy in isotropic turbulence: Resolution effects and scaling in direct numerical simulations. *Phys. Fluids*, 20(4):045108, apr 2008. doi: 10.1063/1.2907227. URL <https://doi.org/10.1063/1.2907227>.
- [30] L. Machiels. Predictability of small-scale motion in isotropic fluid turbulence. *Phys. Rev. Lett.*, 79(18):3411–3414, nov 1997. doi: 10.1103/physrevlett.79.3411. URL <https://doi.org/10.1103/physrevlett.79.3411>.
- [31] G. Nastac, J. W. Labahn, L. Magri, and M. Ihme. Lyapunov exponent as a metric for assessing the dynamic content and predictability of large-eddy simulations. *Phys. Rev. Fluids*, 2(9), sep 2017. doi: 10.1103/physrevfluids.2.094606. URL <https://doi.org/10.1103/physrevfluids.2.094606>.